

Free nanoparticle characterization by optical scattered field analysis: opportunities and perspectives

Marco Potenza · Paolo Milani

Received: 3 July 2014 / Accepted: 27 September 2014 / Published online: 14 October 2014
© Springer Science+Business Media Dordrecht 2014

Abstract Methods for the facile and in-line characterization of size distribution and physical properties of unsupported nanoparticles are of paramount importance for fundamental research and industrial applications. The state-of-the-art free nanoparticle characterization methods do not provide accuracy, high throughput, and operation easiness to support widespread use for routine characterization. In this perspective paper, we describe and discuss the opportunities provided by approaches for nanoparticle characterization based on optical measurements of the field scattered by particles. In particular, we show how insightful is the measure of both the real and the imaginary parts of the field amplitude, a task that has been considered in the past but never had a widespread exploitation. A number of opportunities are generated by this approach, in view of assessing a more efficient characterization and a better understanding of the properties of nanoparticles. We focus our attention on the capability of characterizing nanoparticles of wide interest for applications, considering cases where traditional approaches are not currently effective. Possible exploitations are both in research and in industrial environments: to validate a synthetic process, for example, or for in-line monitoring of a production plant to generate advanced process control

tools, as well as decision-making tools for acting in real time during the production.

Keywords Nanoparticle characterization · Light scattering · Optical properties · Aerosols

Introduction

Anthropogenic and naturally occurring nanoparticles are ubiquitous: they are present in airborne fine powders, aerosols, ocean suspensions and, in general, as a by-product of combustion processes (Murr and Garza 2009; Zhang et al. 2012; Keller et al. 2013). Besides the “incidental” presence of nanoparticle in the atmosphere, water, and soil, industrial manufacturing of “engineered” nanoparticles is revolutionizing large sectors of the worldwide industrial production and distribution chains (Keller et al. 2013; Roco et al. 2011; Pratsinis 2010).

The development of methods for a rapid, non-invasive, and quantitative characterization of unsupported nanoparticles dispersed in fluids (gas or liquid) is of paramount importance for the understanding of their properties, functionality, applicability, and hazards, as well as for industrial production chains based on the manufacturing, handling, and processing of large quantities of nanoparticles with stringent specifications in terms of size and shape (Scheckman et al. 2009; Swihart 2003; Park et al. 2004).

M. Potenza (✉) · P. Milani
CIMAINA and Dipartimento di Fisica, Università di Milano, via Celoria 16, 20133 Milan, Italy
e-mail: marco.potenza@unimi.it

The state-of-the-art free nanoparticle characterization methods do not provide accuracy, high throughput, and operation easiness to support widespread use for routine characterization (Iida et al. 2009; Zelenyuk et al. 2006; Ghosal et al. 2014). As an example, we mention here the case of airborne anthropogenic particles: since the Industrial Revolution, a completely new class of fine powders formed by aggregation of combustion products has been spread into the atmosphere, with environmental and health effects that are still a matter of debate (Ramanathan 1987; Schwartz et al. 2010). Methods to characterize atmospheric aerosols are currently unable to say apart the anthropogenic and the natural fractions over the global scale, as well as to clearly assess the effects of different kind of airborne particles on the global climate (Harvey 1988; Schwartz 1989; Hansen and Lacis 1990; Delmonte et al. 2005; Mahowald et al. 2013; Albani et al. 2014).

Optical methods for particle characterization are in general non-invasive, thus allowing a high degree of compactness, simplicity and reliability in instrumentation. Although optical methods are almost unique in terms of flexibility, simplicity, robustness, sampling speed, etc., nanoparticles are endowed with sizes small enough to prevent the exploitation of methods operating in the visible spectrum range and based upon the determination of form/structure factors, as they are usually measured with traditional scattering techniques.

This perspective paper aims at presenting the opportunities provided by a novel approach for nanoparticle characterization based on optical measurements, in particular, we will concentrate on a whole class of methods based upon the measurement of a couple of independent parameters describing the optical field scattered from particles illuminated by a light beam. These independent parameters can be, for example, both the amplitude and phase of the emerging wavefront, or its real and imaginary parts. We will present and discuss the possibility to assess a more efficient characterization and a better understanding of the properties of nanoparticles by exploiting this approach. We focus our attention on the capability of characterizing nanoparticles of wide interest for applications, considering cases where traditional approaches are not currently effective. Possible exploitations are both in research and in industrial environments: to validate a process, for example, or

for in-line monitoring a production plant to generate advanced process control tools, as well as decision-making tools for acting in real time during the particle production.

We will present the results of numerical simulations since our aim here is to show the kind of information on free particle features obtained from the real and imaginary parts of the scattered field (or the corresponding amplitude and phase), regardless of the specific experimental method to measure them.

Optical methods for nanoparticle characterization: state of the art

Optical methods for characterizing nanoparticles can be divided into two groups: methods for measuring properties of collections of particles and methods for measuring one particle at a time. Their effectiveness, sensibility, and resolution, ultimately depend on the specific parameter (mass, density, shape, etc.) to be characterized.

Traditional particle sizing methods based on light diffraction (or more properly, small angle light scattering, SALS) (Zimm 1948a, b; Wyatt 1993; Gravatt 1971; Cornillault 1972; Ferri et al. 1988) are sensible to particles smaller than the wavelength of light and they can operate with gaseous and liquid samples. Especially when operated with polydisperse samples, they can fail in recovering the size distribution and the resolution becomes very poor [see for example (Bassini et al. 1992)]. Moreover, measurement results are affected by sample composition and the particle shapes (Mishchenko et al. 1999; Borghese et al. 2003). SALS is in principle well suited for in-line applications, however it is fully effective only when applied to the characterization of relatively large particles (from some fractions of the light wavelength, which is some 100 nm). Extensions of the SALS have been successfully adopted in connection with precise measurements of the polarization properties of the scattered radiation (Munoz et al. 2004).

Dynamic light scattering (DLS) works only with particle suspensions in liquids and it has a very high sensibility being capable of measuring sizes smaller than 1 nm. It operates upon collections of a huge number of particles, through the measurement of the light scattered at a given angle (usually 90 deg). The time series of the intensity values measured with a

very high time resolution (typically some 10 ns) deliver the information about the characteristic times of the Brownian diffusive motions, from which the average hydrodynamic radius is extracted (Berne and Pecora 2000; Goldberg 1999). In DLS, the physical quantity to be measured, namely the Stokes–Einstein diffusion coefficient, is independent of the particle composition. This is recovered from the analysis of the characteristic time needed for the scattered intensity to de-correlate, which is inversely proportional to the diffusion coefficient. Actually, this measure is obtained by fitting a single curve, the intensity–intensity time correlation function that can extend upon many decades of time (Berne and Pecora 2000). Particle polydispersity is therefore a strong limitation for DLS, particularly for samples with several modes that generate signals containing different characteristic times and with significantly different scattering cross sections (Aragon and Pecora 1976; Frisken 2001). DLS maintains a dependence on particle shape, usually assumed to be spherical as well. This issue is particularly important for particles larger than the scattered wavelength, when Brownian rotations contribute to the signal in a completely different way (Van Saarloos 1987; Wiltzius 1987; Wiltzius and Saarloos 1987; Lin et al. 1990; Lattuada et al. 2004; Pranami et al. 2010; Potenza et al. 2014).

Among the methods for characterizing single particles in liquid and gas, the most popular and cheap is by far the optical particle counter (OPC), allowing a superior resolution especially at low diameters (roughly speaking, below the wavelength of light) together with a relatively large size range (up to tens of microns) (Sachweh et al. 1998; Heim et al. 2008). The measured parameter by OPC is the intensity of the light scattered by single particles illuminated by a light beam of known intensity. Unfortunately, since the optical cross sections change very rapidly toward the smallest sizes, OPCs pay a price for their very good resolution in dimensions by being limited in sensibility at lower diameters, say at approximately 200–250 nm. Factors limiting the accuracy in determining particle size are the particle composition and shape (Gebhart 1991; Tinke et al. 2008; Liu and Daum 2000; Chylek et al. 1976).

The methods briefly described above can, in principle, be operated in-line for the characterization of nanoparticle size, the determination of other parameters such as shape, index of refraction, etc., is substantially out of reach since the whole information

is squeezed for extracting the size with the highest possible accuracy. In principle, accurate optical characterization combining different measurements (Bantle et al. 1982; Eidhammer 2008), as well as different techniques (Royer et al. 1983; Wang and Sorensen 1999), can assess information about the shape or the refractive index of colloidal suspensions. Although this approach has been used successfully by exploiting commercial devices (Tamborini and Cipelletti 2012), it remains confined to fundamental research.

Recently, a simple method called Nanosight (TM) for the measurement with visible light of nanoparticles down to tens of nm in diameter has been proposed (Hole et al. 2013). Nanosight has been commercialized since 2006 and it had a rapid diffusion for many applications. It measures the diffusion coefficient of single nanoparticles suspended in water from movies taken at a proper angle from the laser beam illuminating the sample. In principle, this could make the difference with the previous methods thanks to the superior sensibility in connection with a relatively simple device. As a matter of fact, several issues are not completely clarified, such as, for example, building a protocol to be shared for obtaining fully compatible results from different instruments operated by different users.

Optical scattered field analysis: a novel approach

A radiation field impinging onto a particle with a size comparable or smaller than the wavelength determines the emission of a new wave usually called scattered wave (Van de Hulst 1957; Bohren and Huffman 1998). The total amount of light removed by scattering from the incoming beam (the so-called extinction, or total, cross section), and the intensity distribution in all directions are the two parameters commonly used for extracting the information about the size (the so-called phase function). The extinction cross section is the sum of the scattering and the absorption cross sections, the latter vanishing for pure dielectric (i.e., non-absorbing) particles. The phase function does contain important information about the scatterers, the most important being their average size. More precisely, the scattered field emerges like a spherical wave from the scatterer: at a distance r and at given angle θ , the field will be described as

$$A(r, \theta) = S(\theta) \frac{\exp[ikr + ikz]}{ikr} A_0, \quad (1)$$

where A_0 represents the amplitude of the incoming plane wave, $k = 2\pi/\lambda$ with λ the light wavelength. $S(\theta)$ is the dimensionless scattering amplitude. In what follows, we will focus our attention on the zero-angle scattering amplitude, $S(0)$.

Other features affecting the wave scattered from a single particle are (1) composition; (2) internal structure; (3) shape. Their influence on the scattered wave properties are much smaller than the size effect (see the extended discussion in (Mishchenko et al. 1999; Borghese et al. 2003) and references therein). The effects of these features on the scattered wave depend upon the size or more specific properties of the particle and are generally quite difficult to obtain.

The novel approach we describe here stems from a further, unconventional analysis of the fundamentals of light scattering. It ultimately relies on the determination of the whole wavefront, namely the real and imaginary parts of the field. This corresponds to measure both the amplitude and the phase of the scattered wavefront, an issue that has always been considered very challenging, if not intractable (Van de Hulst 1957). Nevertheless, it can be obtained with different methods, both for the case of a collection of particles and that of single particles (see “[Characterization approaches](#)” section for details) (Bassini et al. 1997; Batchelder and Taubenblatt 1989; Potenza et al. 2010; Giglio and Potenza 2004, 2005). As a matter of fact, these methods always remained within the border of very narrow scientific applications, with the only exception described in (Batchelder and Taubenblatt 1989; Batchelder and Taubenblatt 1990).

The knowledge of two parameters such as the real and imaginary parts of the field, or the amplitude and phase, represents a huge advantage. It is worth noticing that this phase is different from that recovered with holographic methods, being just the lag between the phase of the incoming and scattered waves. This lag is rigorously defined only in the forward direction, and it does contain information about the scatterer (Potenza et al. 2010): it changes from 0 to $\pi/2$ when increasing the optical thickness of the particle, $s = 2a(m-1)$, from 0 to λ (here a is the radius, m the refractive index relative to the surrounding medium, λ the wavelength of light in vacuum). Since typical values for m are between 1.4 and 2, and for a wavelength of approximately 600 nm, we find that the phase changes appreciably for radii of the order of a

few 100 nm. As a result, within this size range, measuring both the amplitude and phase of the scattered field allows to extract: (1) the scattering cross section (from the field amplitude; (2) the optical thicknesses (from the phase, see the case examples below). Traditional approaches like those described above are based upon one-to-one relationships between either the scattering or the extinction cross section. As mentioned above, these relations depend on the composition/internal structure (which must be assumed a priori). Here we drop this need, thanks to the simultaneous, independent measurement of $\text{Re } S(0)$ and $\text{Im } S(0)$ (or amplitude and phase), which can be related to size and optical thickness: a direct relation of anyone of these quantities with the particle size is ultimately impossible here. On the contrary, by determining both is the key to assess the size of a single particle without any need of knowing its refractive index.

The above argument can be interpreted in terms of the real and imaginary parts of the scattered field. The real part is responsible for the amplitude of the intensity modulations due to interference between the scattered and the transmitted fields, so that it delivers information about the scattering cross section; the imaginary part is directly related to the extinction cross section through the famous Optical Theorem (Van de Hulst 1957; Borghese et al. 2003; Potenza et al. 2010), including both the scattering and absorption effects. Notice that our choice here is to refer directly to the real and imaginary parts of the scattered field, at variance with the usual choice adopted in more theoretical approaches, where proper quantities are defined by normalizing the fields to the geometrical cross sections [see (Borghese et al. 2003) and references therein]. The two choices are fully equivalent, but real and imaginary parts can be directly measured experimentally.

Characterization approaches

Within the optical range, measurements sensitive to the phase of the scattered waves have been devised with early attempts on single particles as described in (Batchelder and Taubenblatt 1989; Bassini et al. 1997). Quite recently, methods simple enough to envisage the possibility of a widespread exploitation for industrial applications have been proven both for

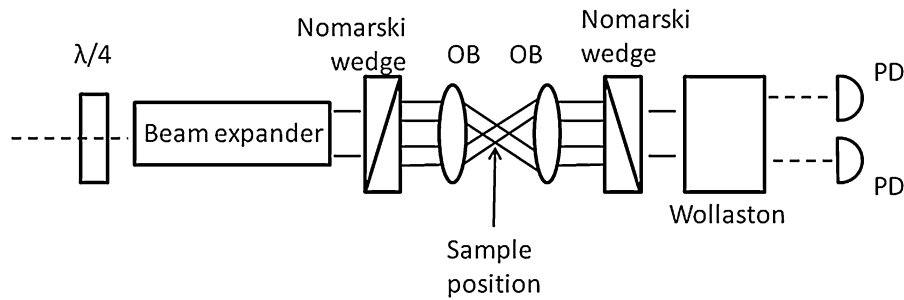


Fig. 1 Schematic of the apparatus for the combined measurement of size and refractive index of single particle described in the text. A polarized laser beam is passed through a quarter wavelength plate, expanded and sent to a Nomarski prism. Two

parallel beams are focused in the sampling region by an objective (OB). The emerging light is collected by a second objective and a Nomarski, passed through a Wollaston prism and the emerging beams are collected by two photodiodes

single particles and collections of particles illuminated by a laser light (Potenza et al. 2010; Giglio and Potenza 2004, 2005). All these methods rely on the interference between the scattered wave and a reference one, thus determining the phase from the interference pattern.

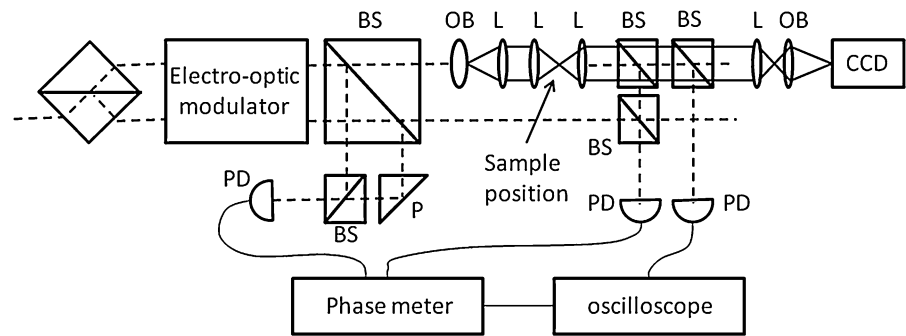
The method described in (Batchelder and Taubenblatt 1989, 1990, 1991) has been conceived with the aim of measuring both size and refractive index of single particles. It relies upon the measure of the forward scattered field generated by a particle illuminated by a focused laser beam, in a scheme exploiting a Nomarski interferometer (see Fig. 1). A laser beam is splitted by a Nomarski prism that generates two parallel beams with perpendicular polarization, both focused at a focal plane in two different positions. Particles are fluxed through the focal plane in a direction perpendicular to the optical axis, some of them passing through the focal regions of the beam. The wave scattered by a particle in one of the focal spots is then collected by a second Nomarski prism that superimposes the two beams again, making them interfere. The emerging field is composed of three components, the two main beams and the scattered wave, which is polarized as one of the two and interferes thus slightly depressing its amplitude. The measure of the intensity of the two polarized components delivers two independent information about the scattered wave: (1) the amount of power removed by the particle, that is directly related to the extinction cross section, and (2) the phase shift between the incoming and the scattered wave, thus giving a complete measurement of the complex field of the scattered wave. The method has been patented (Batchelder and Taubenblatt 1990) due to its suitability to be operated for in-line operations.

The method has been proven to be effective in measuring polystyrene particles with diameters from approximately 100 to 400 nm, corresponding to a range of $\text{Re } S(0)$ which extends from 10^{-3} up to 1.

In (Bassini et al. 1997), a Mach-Zehnder-type interferometer was exploited for measuring the phase lag of the wave scattered from single polystyrene spheres on the surface of a glass slide, and the simultaneous measure of the power removed from the beam allowed to get the complete information on the field (see Fig. 2). In practice, a He-Ne laser beam was 50 % splitted into two beams, one of which was frequency shifted by 100 kHz, interfered with half of the reference and the beating intensity monitored by a fast photodiode. The reference beam was tightly focused onto the test particle, and the superposition of the transmitted and the scattered waves 50 % collected by a microscope objective and 50 % collected by a photodiode to give an intensity monitor. The light was then interfered with the frequency-shifted beam and the intensity monitored by a second photodiode. Actually, the method was effective just by performing differential measurements, in order to get rid of unavoidable perturbations of the optical paths. Measurements were in excellent agreement with the theoretical expectations within a range of diameters from 200 nm up to 1 μm (corresponding to $\text{Re } S(0)$ from 10^{-2} up to 3) for polystyrene spheres.

In (Potenza et al. 2010; Giglio and Potenza 2004, 2005), the same issue has been addressed by adopting a very convenient optical scheme, based upon the self-reference interference in which the reference wave is just the transmitted one, in a self-reference interference scheme that is very similar to in-line holography (Goodman 1996). The method described in (Potenza

Fig. 2 Schematic of the apparatus for the measurement of the phase lag of the scattered field of single particle described in the text. *BS* beam splitters, *OB* objectives, *L* lenses, *PD* photodiodes, *P* prism. The sample is firmly positioned as indicated by the *arrow*



et al. 2010) operates through a statistical analysis of the interference pattern generated by a collection of particles, relying on the properties of Fourier transforming two dimensional chirped functions. The core of the method stems from recent applications developed for extracting statistical information from images taken just downstream a random sample illuminated by a coherent field in a scheme that is reminiscent of the traditional in-line holography, converting easy image analysis procedures in fully effective scattering measurements (Giglio et al. 2000; Brogioli et al. 2002; Mazzoni et al. 2013). The size range here is between 200 nm and 5 μm diameter (polystyrene spheres), and the accordance of the experimental data with theoretical expectations is excellent. In (Giglio and Potenza 2004, 2005) the amplitude and phase are measured just from the visibility and position of the fringes within patterns formed by interference between a single spherical wave and the transmitted plane wave. A digital hologram is recorded in a very divergent beam, thus picking up the lowest order interference fringes that can be automatically processed to extract the phase lag. These schemes allow for in-line exploitation of these self-interference methods, and appreciably extends the accessible range at smaller sizes.

Case examples

The cases presented in the following mainly deal with the properties of spherical particles, or to particles that can be approximated to spherical structures within a good degree of approximation. This choice is motivated by the huge number of applications and processes requiring the characterization of particles

formed and/or dispersed in liquids, so that the surface tension acts as a strong limiting factor for asymmetric shapes. Nevertheless, in many cases nanoparticles are not spherically shaped, such as for example the case of ground powders, clay particles, needles, etc. Therefore, we will also address the case of asymmetric scatterers, and get insight into the additional complexity thus introduced into the scattering properties: asymmetric particles need to explicitly consider their orientation, which is an additional degree of freedom on top of the shape itself.

In the following sections, we will first show results for the scattered fields obtained for spheres of different materials (“Nanoparticles of unknown composition” in section), thus studying the sensibility to changes in the refractive index. To do this, we will rely on the exact Mie theory (Van de Hulst 1957; Bohren and Huffman 1998), adopting the Lompado Mathematica (TM) code, which has been extensively compared to several analytical and numerical approaches (see for example Penttila et al. 2007). In “Clusters of nanoparticles” section, we describe the scattered fields from clusters of nanoparticles such those typically formed during colloidal aggregation processes, bringing to fractal structures. We adopt here the simple model for scattering by large objects with refractive index close to unity, described in (Van de Hulst 1957), and properly adapted to this aim (see below). Then we will concentrate on the effects determined by spherical scatterers with a coating (“Coated spherical particles” in section) and will elucidate the effects caused by non-spherical objects (“Non spherical particles” in section). In order to evaluate the scattered fields in these complex situations, we adopted a numerical approach based upon the discrete dipole

approximation method (DDA, see below) (Purcell and Pennypacker 1973).

Numerical simulations have been performed through the Amsterdam Discrete Dipole Approximation code (ADDA) (Yurkin and Hoekstra 2011), that is widely considered as a good reference. DDA is a very general method for calculating scattering from a particle of a given geometry and composition. It has been introduced since long ago in astrophysics for similar purposes (Purcell and Pennypacker 1973). The basic idea is to divide the particle into small cubical domains and to replace them by point-like dipoles. The interactions between dipoles are then calculated numerically on the basis of the integral equation for the electric field. For an extensive review of the issues dealing with the practical implementation of the integral equations, see (Yurkin and Hoekstra 2007). The ADDA code is now a widespread implementation of the method, developed in C since 1990 by the Amsterdam group (Hoekstra et al. 1998, 2001). The code has been compared to other numerical codes and the analytical Mie code as well by the authors, as described in (Yurkin et al. 2007; Penttila et al. 2007).

Nanoparticles of unknown composition

This example is based on the possibility to extract information from a proper characterization of the scattered light in a relatively simple case of spherical particles of different materials. Although it could be considered a minor advantage in comparison with the cases we will introduce later on, we discuss it at first because it constitutes a kind of benchmark for this approach, the refractive index being responsible for the change in the optical thickness. The sensibility to the refractive index of single particles immediately brings to the capability of measure, or at least to estimate, it. This implies a better knowledge of the scattering process, which can be easily turned into a better determination of size, for example, without any need of independent knowledge of the particle material as it is for traditional methods.

We compare the scattered fields from water suspensions of spherical particles uniformly endowed with the following refractive indexes: $n = 1.45$, 1.6 , 2.1 . We also include a couple of cases of great interest here, that of absorbing particles, so that we have $n = 1.6 + 0.25i$, $1.6 + 0.5i$ [where i is the imaginary unit to quantify the absorption of a material: here we

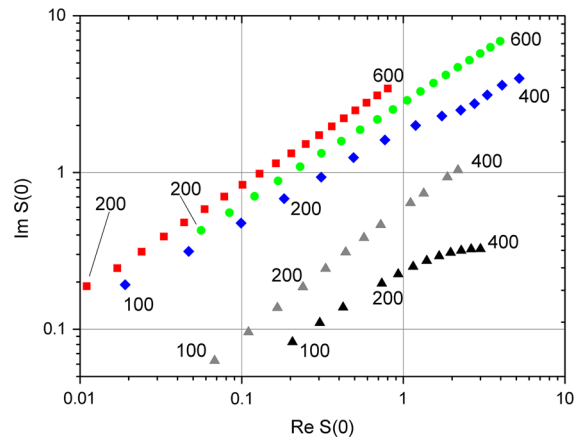


Fig. 3 The fields scattered by spheres of different materials, as discussed in the text. Different data sets refer to different refractive index (from top to bottom, 1.09, 1.2, 1.58, $1.2 + 0.2i$, $1.2 + 0.4i$). Numbers indicate the diameter of a spherical particle (in nm) scattering the given field

adopt the general notation for the positive imaginary part, as it is done in (Bohren and Huffman 1998), at variance with (Van de Hulst 1957)]. More practically, examples of materials with these indexes are, respectively, the common copolymer poly(lactic-co-glycolic) acid (a widely used polymer, approved by the FDA), polystyrene (typical for calibrating instrumentation), ceria oxide (largely used in manufacturing industries). Regarding the absorbing particles, the latter value is typical for black carbon, while the former is just set to give an intermediate absorption. For the sake of completeness, the refractive indexes relative to water are, respectively, 1.09, 1.2, 1.58, $1.2 + 0.2i$, and $1.2 + 0.4i$. Mie theory has been adopted here to evaluate the complex scattered fields.

The real and imaginary parts of the fields are represented in Fig. 3 for a wavelength of 632.8 nm (He–Ne laser). Different materials bring to fields that identify different lines within the plot. More precisely, fields from spheres with $n = 1.45$ and $n = 1.6$ have been represented for a radius range 200–600 nm (red squares and green circles respectively). For the other cases, radii between 100 and 400 nm have been considered. This difference in the size ranges is the result of the strong dependence of the fields upon the composition of the particles. It implies a different sensibility of the method depending on the material, which is a novelty here. In fact, since traditional methods generally measure only the scattered

intensity, recovering the size distribution needs to assume a value for the refractive index.

Notice that increasing the size determines larger scattered amplitudes (left-bottom corner: small sizes; top-right corner: large sizes); for a given real part, increasing the refractive index makes the imaginary part to decrease. A relationship as simple as that does not exist by fixing the size, as well as just the real part of the scattered field. The size affects both $\text{Re } S(0)$ and $\text{Im } S(0)$.

Figure 1 shows that no other information is necessary to determine both the size and the refractive index of each measured particle, so that the size distribution of a collection of particles can be obtained without any a priori assumption (at least for spherical particles: see below). With the increasing refractive indexes, the changes in the scattered fields decrease. From one side, this reduces the resolution in determining the index itself. From the other side, a precise knowledge of it is less important in recovering the size, making the method very robust in terms of determining the particle size distribution.

A separate issue is represented by the absorbing particles: here, the sensibility of the fields to the imaginary part of the refractive index appears to be rampant. This allows to recognize undoubtedly the presence of such particles in a given suspension. By the same token, this makes the estimate of the real part of the refractive index much more difficult, if not impossible. Again, this does not limit the capability of measuring the size.

Clusters of nanoparticles

Aggregation of nanoparticles suspended in a fluid is of fundamental importance both for scientific and industrial applications. Aggregation is usually described on the basis of one of the two limiting phenomena, describing the two extremes of the real processes: either the Brownian diffusion of particles toward the aggregates (Witten and Sander 1983), namely the diffusion-limited aggregation processes, or the sticking probability (Meakin 1983) (see (Weitz et al. 1985; Veen et al. 2012), where the activation barrier of the sticking potential has been changed). The latter process, known as reaction-limited aggregation, is determined by the interaction strength, including effects of the activation barrier in the sticking of the particles. As a matter of fact, even for strong interactions, aggregates grow with characteristics typical of the reaction limited processes due to

external effects on the whole aggregate (Ball 1987; Lin et al. 1989a, b, 1990). The information contained in the aggregates is then changed, making very difficult, if not impossible, to measure the interaction strength from the features of aggregates. Here we show how the knowledge of the complex scattered field could be important for obtaining information from systems forming fractal aggregates.

Thanks to very general rules, a simple analytical description can be adopted for the fractal aggregates. We describe the aggregates as spherical objects with uniform polarizability. This allows to obtain a good approximation for the scattered field in the forward direction within the size range considered here, which in connection with the relative refractive index very close to 1 guarantees the Rayleigh-Gans approximation to be well satisfied (Van de Hulst 1957). For describing the aggregates, we refer to the traditional notation adopted in colloidal physics: M is the number of monomers contained into a given aggregate of volume V , so that $N = M/V$ is the number density of monomers within the aggregate. The monomer radius, a , and the gyration radius of the aggregate, R , are related through the following relation:

$$M = \left(\frac{R}{a}\right)^d, \quad (2)$$

where d is the fractal dimension of the aggregate. As a result, the number density of monomers within the aggregate (assumed to be spherical) will be simply given by

$$N = \left(\frac{R}{a}\right)^d \frac{3}{4\pi} R^{-3}. \quad (3)$$

Now we can obtain the properties of the aggregate from that of the monomers. By applying the Lorentz-Lorenz formula (Van de Hulst 1957; Bohren and Huffman 1998), if μ indicates the refractive index of the monomers,

$$\frac{3(\mu^2 - 1)}{(\mu^2 + 2)} = 4\pi N_0 \alpha, \quad (4)$$

where N_0 is the number density of molecules with polarizability α within the monomer. By assuming that $(\mu - 1) \ll 1$ as it is fully acceptable in our case, one finds

$$\mu - 1 = 2\pi N_0 \alpha. \quad (5)$$

By exploiting the same argument for the aggregates, the refractive index m can be obtained as

$$m - 1 = 2\pi V_0 N_0 \alpha, \tag{6}$$

where V_0 is the volume of each monomer. By assuming spherical monomers, we immediately obtain

$$m - 1 = \left(\frac{R}{a}\right)^{d-3} (\mu - 1). \tag{7}$$

As a result, we can express the refractive index of the aggregate of size R as a function of the refractive index of the monomers of index μ and radius a .

A convenient approximation of the exact Mie theory can be done by assuming that, if k is the wavevector and $x = kR$:

$$m - 1 \ll 1 \tag{8a}$$

$$2kR(m - 1) \ll 1 \tag{8b}$$

(the so-called Rayleigh-Gans conditions). These conditions are usually well satisfied during a colloidal aggregation process. The expression for the forward scattered wave can then be reduced to the simple form (Van de Hulst 1957):

$$S(0) = x^2 K(i\rho), \tag{9}$$

where $\rho = 2x(m - 1)$ is the optical thickness of the aggregate, $x = kR$, and the function K results from the integration across the sphere:

$$K(w) = \frac{1}{2} + \frac{e^{-w}}{w} + \frac{e^{-w} - 1}{w^2}. \tag{10}$$

This result allows to evaluate the scattered field from the aggregates. It depends upon the monomer radius a , the aggregates gyration radius R , and the fractal dimension d . In Fig. 4, the cases $d = 1.8$ and $d = 2.1$ are represented (crosses and open squares respectively), compared to the scattered fields obtained from the Mie theory for compact spheres (solid circles). Here the monomer radius has been assumed to be $a = 50$ nm, and the growth up to a gyration radius $R = 1 \mu\text{m}$ is represented.

Finally, by introducing the optical thickness of the monomer, $\rho_0 = 2x_0(\mu - 1)$, one obtains

$$\frac{\rho}{\rho_0} = \left(\frac{R}{a}\right)^{d-2} \tag{11}$$

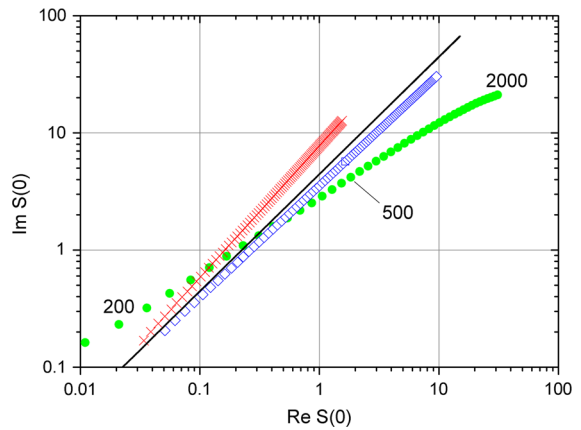


Fig. 4 The expected fields scattered by fractal aggregates formed by spherical monomers 50 nm in radius, up to a gyration radius $R = 1 \mu\text{m}$. Fractal dimensions $d = 1.8$ (red crosses) and $d = 2.1$ (blue open squares) are represented. The straight line indicates the discriminant expected for $d = 2$ on the basis of the simple model presented in the text. For comparison, the fields scattered by compact, spherical polystyrene particles are represented (green circles). Numbers indicate the radius of the spherical particles in nm. (Color figure online)

irrespective of the refractive index of the monomer. This clearly indicates how the measure of the real and imaginary parts of the scattered field is useful for studying the aggregates. In fact, the value 2 for the fractal dimension determines whether the optical thickness increases or decreases with the increasing aggregate size R . By expanding in power series the real and imaginary parts of the scattered field, one obtains $\text{Re}(S(0)) = x^2 \rho^2 / 8$, $\text{Im}(S(0)) = x^2 \rho / 3$. For $d = 2$, this corresponds to a straight line with derivative $\rho_0 8/3$ in the complex field, which is represented by a solid line in Fig. 5. For $d > 2$, the aggregates will determine a real part of the scattered field increasing faster than the imaginary, while the $d < 2$ case corresponds to a faster increase of the imaginary part. By monitoring the aggregation process, it will be possible to get insight into the aggregates in a completely new way, by determining the speed of growth and the fractal dimension.

In Fig. 4, we represent the fields expected for fractal aggregates formed by spherical monomers 50 nm in radius, up to a gyration radius $R = 1 \mu\text{m}$. Here red crosses indicate the fields scattered by aggregates with a fractal dimension $d = 1.8$, open blue squares for $d = 2.1$. The solid line gives the expected fields for $d = 2$. Comparing to spheres

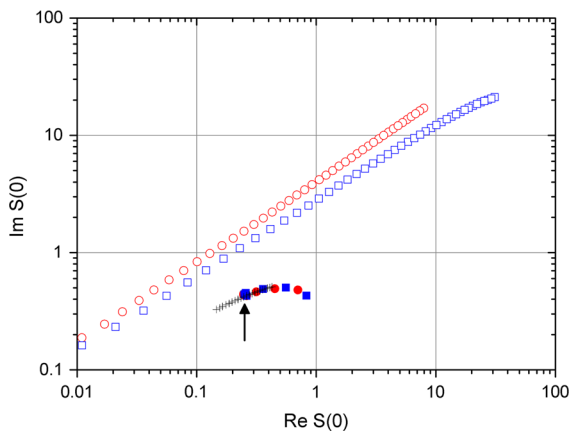


Fig. 5 The fields scattered by Ag nanospheres 100 nm in diameter coated with polymeric layers of different thickness (see text). The field scattered from single Ag spheres is indicated by the arrow. Solid symbols represent the fields scattered by coated particles, as discussed in the text. Small crosses are the fields scattered by Ag cores with a distribution of sizes. Open symbols represent the fields from spheres made of pure polymer (red circles $n = 1.45$; blue squares $n = 1.60$). (Color figure online)

(green circles), it is evident that it is possible to recognize the aggregate nature of a suspension of clusters with an extended size distribution by analyzing the slope of the curves in Fig. 4. Moreover, a precise measure of this steepness gives a measure of the fractal dimension that is absolutely independent of any other known method.

A further possibility will be opened by monitoring the growth of clusters composed by just two particles (dimers), which are small enough not to be so much affected by external effects such as convection, settling, etc. This would preferably require monodisperse particles, in such a way that the presence of a few dimers is easily measurable, thus recovering the information about the early stages of an aggregation process. Irrespectively of the knowledge of the starting monomers, this method relies on the fact that the maximum change in the scattering field occurs just when dimers are formed. Real and imaginary parts are changed accordingly. Moreover, properties of symmetry are changed, so that the random orientations will determine a spread in the fields that can be exploited as a signature of the presence of dimers. This approach could be useful for measuring the interaction potential determining aggregation, an issue of superior interest for the whole bottom-up approach to build nano- and micro-structures.

Notice that, at variance with the rest of this work, this result has been obtained on the basis of a model, and does not directly come from evaluating the fields scattered by each single particle.

Coated spherical particles

Particularly interesting are scatterers constituted by spherical particles with a coating. This is a case of the major importance for industrial applications in medicine, for example, where a given nanoparticle must be coated with a polymer, which may be dissolved by changing macroscopic parameters such as pH or temperature (Petros and DeSimone 2010; Oerlemans et al. 2010; Silva et al. 2013). This topic has been largely studied from a theoretical point of view (Mishchenko et al. 1999; Borghese et al. 2003), especially for assessing the effects of coating from spectral features. Here we address this issue in the simplest case, a given spherical core with a concentric, uniform coating. In the next section we will go deeper into the effects of a structure characterizing either the coating or the core, or both. As an example, we focus our attention on cores composed by Ag spheres. This choice is dictated by two different issues: (1) the relevance of silver nanoparticles in industrial and biotechnological applications (Locatelli et al. 2012); (2) the fact that the surface plasmon of Ag has a maximum in the green, that means we can treat the refractive index of Ag quite reasonably in the red, where the effect of the plasmons will not be important. Here we will assume a value for the refractive index for Ag $n = 0.3 + 3.66i$ (Van de Hulst 1957). This value could be questioned, or other values considered more correct (see for example (Palik 1985), who gives $0.13 + 3.99i$ at our wavelength). Nevertheless, as it will become clear soon, this choice will not really affect the discussion since the actual complex field of the Ag particles exploited as the core can be directly measured and the effect of coating assessed on the basis of what is essentially a kind of differential measurement. We also fix the diameter of the Ag core to be 100 nm. The effect of coating has been evaluated for two different refractive indexes $n = 1.45$ and $n = 1.6$ (see “Nanoparticles of unknown composition” section). Also the effect of thickness have been studied, for diameters of 105, 110, 120, 150, and 200 nm.

Results are plotted in Fig. 5 (red: $n = 1.45$; blue: $n = 1.6$), the position of the Ag core particles is indicated by an arrow, and the thickness of the coating increases upon moving rightward. Notice that for thickness larger than 10 nm, the coating becomes detectable, especially if a direct comparison is possible with the naked Ag spherical cores. Of course, this sensibility is dependent on the quality of the Ag spheres, which may spread the results around the expected position. In order to quantify this effect, in Fig. 5, we have plotted a number of small crosses representing the fields of Ag spheres with sizes distributed around 100 nm with a standard deviation of 10 %. In this case, a coating thicker than 25 nm is actually detectable for a 100-nm-diameter core.

In Fig. 5, we also plot the fields scattered from uniform spheres with the same refractive indexes of the coating (open symbols), over a wide range of sizes. This shows the potentiality of the method to distinguish spheres containing the Ag core from spheres made of pure polymer that can naturally grow during the coating process. Saying apart these two species is an unresolved issue with traditional methods, while this approach shows to be highly reliable: coated spheres are segregated within a region of the plot that is completely separated from that occupied by spheres of pure polymer.

Non spherical particles

Extensive theoretical approaches describing particles with non-spherical shapes have been presented in (Mishchenko et al. 1999; Borghese et al. 2003; Purcell and Pennypacker 1973; Hoekstra and Sloot 1994) (see also references therein). Here we analyze how the shape affects the scattered fields, demonstrating that the largest influence is given by aspect ratios departing from 1, almost irrespectively of the fact that objects are oblate or prolate. Beyond the obvious departure from symmetry of the scattered field, dropping the spherical assumption immediately introduces the additional degree of freedom represented by orientation. The effects of shape and orientation ultimately depend on the particles size, making the most striking difference for particles of some hundreds of nanometers or larger. Finally, we show that pronounced aspect ratios change the scattered fields in a way that is somehow similar to what is obtained with a distribution of refractive indexes.

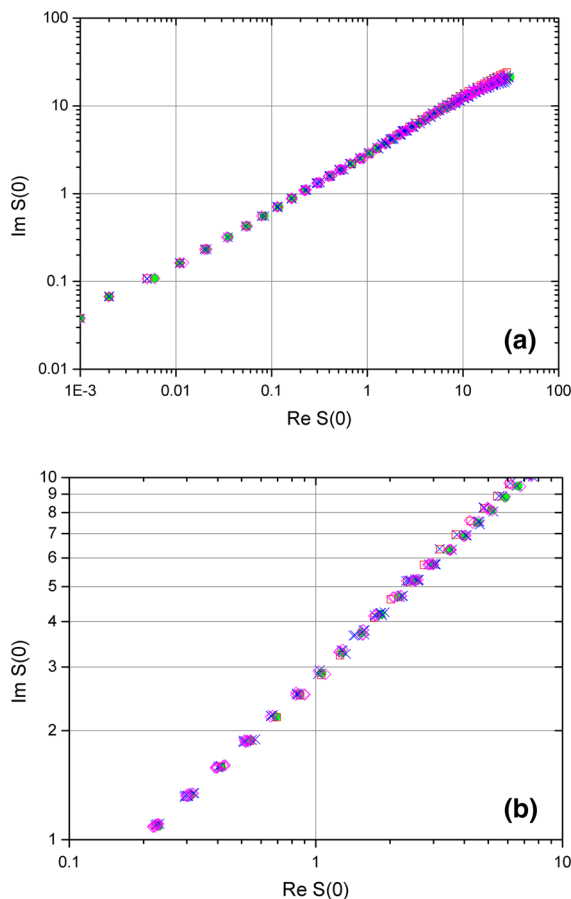


Fig. 6 Fields scattered by particles having different shapes and the same aspect ratio. In **a** we show the fields for a range of radii from 50 to 500 nm for spheres (green circles), cubes (red squares), cylinders (blue crosses), and prisms (magenta diamonds). In **b** a detail of the previous plot is represented, to better show the differences between the fields for radii from 140 nm up to 350 nm. (color figure online)

Here we refer to sizes in terms of the so-called equivalent radius, i.e., the radius of the spheres with the same volume of the given particle. This permits to set a uniform size range and to evaluate how the same volume packed into compact objects with different shapes affects the scattered fields. First, we show that the fields are almost unchanged for objects with many different shapes but with the same aspect ratio. Results for spheres (green circles, almost hidden by the other symbols), cubes (red squares), cylinders (blue crosses), and prisms (magenta diamonds) are compared in Fig. 6 for orientations at random. Irrespective of the shape and orientation, the fields are

concentrated along a very thin line, which position depends on refractive index as shown in Fig. 3.

We consider objects which aspect ratio is appreciably different from 1 showing some cases representative of a much larger class of similar shapes. We first analyze the case of platelets with aspect ratio 0.2, and needles with aspect ratio 5. These are typical examples of what happens for oblate and prolate objects of many different shapes, as we directly checked for cylinders, prisms with several faces, ellipsoids. Here we show results for pentagonal prisms, the other shapes essentially bringing to the same results, also from a quantitative point of view. In Fig. 7a, crosses indicate the fields obtained from 1,000 numerical simulations of platelets with equivalent radii from 50 to 500 nm, randomly oriented. Figure 7b has been obtained with needles of pentagonal section under the same conditions. The comparison with Fig. 6 clearly shows the importance and the potentiality of our approach: depending on the orientation, the field changes in both the real and imaginary parts. More precisely, the spread of the fields depend on the aspect ratio, being larger for platelets than needles. Moreover, according to what is discussed in “[Optical scattered field analysis: a novel approach](#)” section, the spread directly comes from the combined measures of both the optical thicknesses and the extinction cross section, that are proportional to the imaginary and the real parts of the field. For example, when platelets are oriented face on (with respect to the incoming light) they show the maximum cross section with a limited optical thickness. Conversely, for the edge on case the cross section is reduced and the optical thickness increased. As a matter of fact, it is evident from Fig. 7a that fields group along two main sequences, just corresponding to the regions where fields come from particles oriented as described before. It is also noticeable that fields are not uniformly distributed in between. For comparison, spheres have been also reported in both plots (solid circles): they are barely visible in the plot, being very close to the fields from face-on oriented objects.

This result shows the importance of accessing the field, traducing in both extinction and scattering cross sections changing by a factor 2 or 3. By contrast, a measure of the size distribution in this case would bring much less information. Just to make an example, in the case of airborne particles it appears very clear that the size distribution would not bring the correct

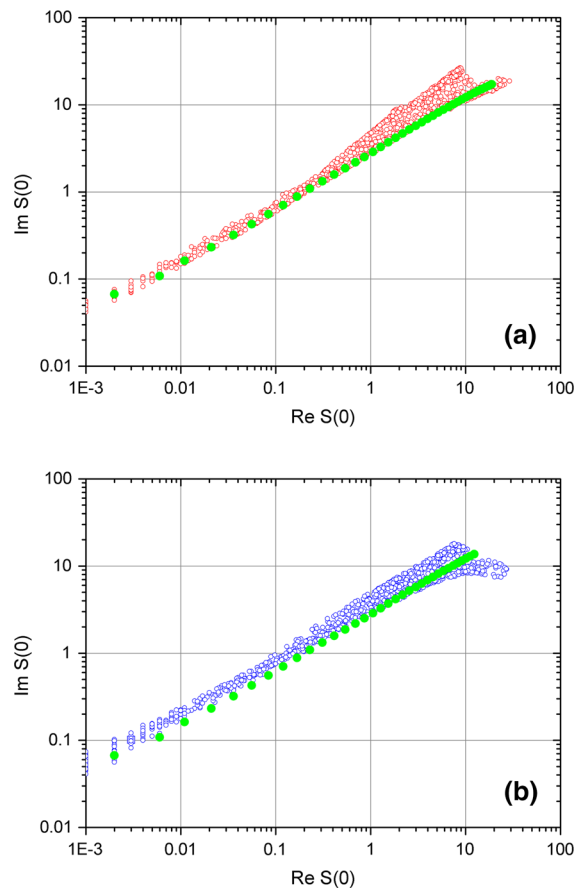


Fig. 7 Fields scattered by particles having different shapes with aspect ratios appreciably far from 1. *Red crosses* and *blue circles* indicate fields scattered by cylindrical platelets (a) and needles (b) with aspect ratio 5, randomly oriented. Volume equivalent radii span the range 50–500 nm. For comparison, the results for spheres obtained for the same range of sizes is reported in both plots (*green circles*; see Fig. 6). (Color figure online)

information in terms of the optical properties of the aerosol. On the other side, the measure of both the field components in principle could deliver precious information about the particle shape, especially in the size range from 100 nm up to 500 nm equivalent radius. In particular when one material is considered, and the general shape can be easily guessed, the spread shown in Fig. 7 allows to get information about the aspect ratio.

Conclusions

We have presented and discussed a novel approach for the efficient characterization of unsupported

nanoparticles through light scattering methods. This approach is based upon the measurement of real and imaginary parts of the scattered field independently, an issue that can be viable thanks to recent developments of optical and detection methods.

We foresee that this approach will bring to the implementation of characterization methods based on cheap and portable devices, capable of working in line and producing reliable results in real time. This will also allow to operate in environments such as industrial plants, environmental monitoring stations, on top of the more natural applications in research laboratories, clean rooms, spacecrafts. The long-term breakthrough of these methods will be a widespread monitoring of micro- and nano-particulates in public and work environments.

References

- Albani S et al (2014) Improved dust representation in the community atmosphere model. *J Adv Model Earth Syst*, accepted
- Aragon SR, Pecora BJ (1976) Theory of dynamic light scattering from polydisperse systems. *J Chem Phys* 64:2395–2404
- Ball RC, Weitz DA, Witten TA, Leyvraz F (1987) Universal kinetics in reaction-limited aggregation. *Phys Rev Lett* 58:274
- Bantle S, Schmidt M, Burchard W (1982) Simultaneous static and dynamic light scattering. *Macromolecules* 15:1604–1609
- Bassini A et al (1992) Optical particle sizer based on the Chahine inversion algorithm. *Opt Eng* 31:1112–1117
- Bassini A et al (1997) Interferometric system for precise sub-micrometer particle sizing. *Appl Opt* 31:8121–8127
- Batchelder JS, Taubenblatt MA (1989) Interferometric detection of forward scattered light from small particles. *Appl Phys Lett* 55:215–217
- Batchelder JS, Taubenblatt MA (1990) Measurement of size and refractive index of particles using the complex forward-scattered electromagnetic field. US Patent 547735
- Batchelder JS, Taubenblatt MA (1991) Measurement of the size and refractive index of a small particle using the complex forward-scattered electromagnetic field. *Appl Opt* 30:4972–4979
- Berne BJ, Pecora R (2000) *Dynamic light scattering*. Dover, New York
- Bohren CF, Huffman DR (1998) *Absorption and scattering of light by small particles*. Wiley-VCH, Berlin
- Borghese F, Denti P, Saija R (2003) *Scattering from model nonspherical particles*. Springer, Berlin
- Broglioli D, Vailati A, Giglio M (2002) Heterodyne near field scattering. *Appl Phys Lett* 81:4109–4112
- Chylek P, Grams GW, Pinninck RG (1976) Light scattering by irregular randomly oriented particles. *Science* 193:480–482
- Cornillault J (1972) Particle size analyzer. *Appl Opt* 11:265–268
- De Temmerman P-J, Van Doren E, Verleysen E, Van der Stede Y, Francisco MAD, Mast J (2012) Quantitative characterization of agglomerates and aggregates of pyrogenic and precipitated amorphous silica nanomaterials by transmission electron microscopy. *J Nanobiotech* 10:24
- Delmonte B et al (2005) Ice core evidence for secular variability and 200-year dipolar oscillations in atmospheric circulation over East Antarctica during the Holocene. *Clim Dyn* 24:641–655
- Eidhammer T (2008) Determination of index of refraction and size of supermicrometer particles from light scattering measurements at two angles. *J Geoph Res* 113:D16206
- Ferri F et al (1988) Low-angle elastic light scattering study of diffusion-limited aggregation. *Europhys Lett* 7:599–604
- Friskin B (2001) Revisiting the cumulant method for the analysis of dynamic light scattering data. *Appl Opt* 40:4087–4091
- Gebhart J (1991) Response of single-particle optical counters to particles of irregular shape. *Part Part Syst Charact* 8(1991):40–47
- Ghosal S, Weber PK, Laskin A (2014) Spatially resolved chemical imaging of individual atmospheric particles using nanoscale imaging mass spectrometry: insights into particle origin and chemistry. *Anal Methods* 6:2413–2792
- Giglio M, Carpineti M, Vailati A (2000) Space intensity correlations in the near field of the scattered light: a direct measurement of the density correlation function $g(r)$. *Phys Rev Lett* 85:1416–1419
- Giglio M, Potenza MAC (2004) A method for measuring properties of particles by means of interference fringe analysis and corresponding apparatus. Patent IT TO20040100; PCT/IB2005/000411
- Giglio M, Potenza MAC (2005) Process for measuring properties of particles and corresponding apparatus. Patent PCT/IT2005/000362
- Goldburg WI (1999) Dynamic light scattering. *Am J Phys* 67:1152–1160
- Goodman JJ (1996) *Introduction to fourier optics*. McGraw-Hill, New York
- Gravatt CC (1971) The applications of light scattering. *Appl Spectrosc* 25:509–516
- Hansen JE, Lacis AA (1990) Sun and dust versus greenhouse gases: an assessment of their relative roles. *Nature* 346:712–719
- Harvey LDD (1988) Climatic impact of ice-age aerosols. *Nature* 334:333–334
- Heim M et al (2008) Performance evaluation of three optical counters with an efficient “multimodal” calibration method. *Aerosol Sci* 39:1019–1031
- Hoekstra AG, Sloop PMA (1994) New computational techniques to simulate light-scattering from arbitrary particles. *Part Syst Charact* 11:189–193
- Hoekstra AG, Grimminck MD, Sloop PMA (1998) Large scale simulations of elastic light scattering by a fast discrete dipole approximation. *Int J Mod Phys C* 9:87–102
- Hoekstra AG et al (2001) Radiation forces in the discrete-dipole approximation. *J Opt Soc Am* 18:1944–1953
- Hole P et al (2013) Interlaboratory comparison of size measurements on nanoparticles using nanoparticle tracking analysis (NTA). *J Nanoparticle Res* 15:2101–2113
- Iida K, Stolzenburg MR, McMurry PH (2009) Effect of working fluid on sub-2 nm particle detection with a laminar flow ultrafine condensation particle counter. *Aerosol Sci Technol* 43:81–96

- Keller AA, McFerran S, Lazareva A, Suh S (2013) Global life-cycle releases of engineered nanomaterials. *J Nanopart Res* 15:1692
- Lattuada M, Wu H, Morbidelli M (2004) Rotational diffusivity of fractal clusters. *Langmuir* 20(20):5630–5636
- Lin MY et al (1989a) Universality in colloidal aggregation. *Nature (London)* 339:360–362
- Lin MY, Lindsay HM, Weitz DA, Klein R, Ball RC, Meakin P (1989b) Universality of fractal aggregates probed by light scattering. *Proc R Soc Lond A* 423:71–87
- Lin MY, Lindsay HM, Weitz DA, Klein R, Ball RC, Meakin P (1990) Universal reaction limited colloid aggregation. *Phys Rev A* 41:2005–2020
- Liu Y, Daum PH (2000) The effect of refractive index on size distributions and light scattering coefficients derived from optical particle counters. *J Aerosol Sci* 31:945–957
- Locatelli E et al (2012) Lipophilic silver nanoparticles and their polymeric entrapment into targeted-PEG-Based micelles for the treatment of glioblastoma. *Adv Healthcare Mater* 1:342–347
- Mahowald N et al (2013) The size distribution of desert dust aerosols and its impact on the Earth system. In press on *Aeolian Research*
- Mazzoni S et al (2013) SODI-COLOID: a combination of static and dynamic light scattering on board the International Space Station. *Rev Sci Instrum* 84:043704
- Meakin P (1983) Diffusion-controlled cluster formation in 2–6 dimensional space. *Phys Rev A* 27:1495–1507
- Mishchenko MI, Hovenier JW, Travis LD (eds) (1999) *Light scattering by nonspherical particles: theory, measurements, and applications*. Academic, San Diego
- Munoz O et al (2004) Scattering matrices of volcanic ash particles of Mount St. Helens, Redoubt, and Mount Spurr Volcanoes. *J Geophys Res* 109:D16201
- Murr LE, Garza KM (2009) Natural and anthropogenic environmental nanoparticulates: their microstructural characterization and respiratory health implications. *Atmos Environ* 43:2683–2692
- Oerlemans C et al (2010) Polymeric micelles in anticancer therapy: targeting, imaging and triggered release. *Pharm Res* 27(12):2569–2589
- Palik ED (1985) *Handbook of optical constants of solids*. Academic Press, Boston
- Park J, An K, Hwang Y, Park J-G, Noh H-J, Kim J-Y, Park J-H, Hwang N-M, Yeon T (2004) Ultra-large-scale syntheses of monodisperse nanocrystals. *Nat Mater* 3:891–895
- Penttila A et al (2007) Comparison between discrete dipole implementations and exact techniques. *JQSRT* 106:417–436
- Petros RA, DeSimone JM (2010) Strategies in the design of nanoparticles for therapeutic applications. *Nat Rev Drug Discov* 9:615–627
- Potenza MAC et al (2010) How to measure the optical thickness of scattering particles from the phase delay of scattered waves: application to turbid samples. *Phys Rev Lett* 105:193901
- Potenza MAC et al (2014) Dynamics of colloidal aggregates by critical Casimir forces. *Eur Phys Lett* 106:68005
- Pranami G, Lamm MH, Vigil RD (2010) Molecular dynamics simulation of fractal aggregates diffusion. *Phys Rev E* 82:051402
- Pratsinis SE (2010) Aerosol-based technologies in nanoscale manufacturing: from functional materials to devices through core chemical engineering". *AIChE J* 56:3028–3035
- Purcell EM, Pennypacker CR (1973) Scattering and adsorption of light by nonspherical dielectric grains. *Astrophys J* 186:705–714
- Ramanathan V (1987) The role of Earth radiation budget studies in climate and general circulation research. *J Geophys Res* 92:4075–4095
- Roco MC, Mirkin CA, Hersam MC (2011) Nanotechnology research directions for societal needs in 2020: summary of international study. *J Nanopart Res* 13:897–919
- Royer A, De Angelis M, Petit JR (1983) A 30000 year record of physical and optical properties of microparticles from an East Antarctic ice core and implications for paleoclimate reconstruction models. *Clim Chang* 5:381–412
- Sachweh B et al (1998) Performance evaluation of three optical counters with an efficient “multimodal” calibration method. *Aerosol Sci* 29:1075–1086
- Scheckman J, McMurry PH, Pratsinis SE (2009) Rapid characterization of agglomerate aerosols by in situ mass mobility measurements. *Langmuir* 25:8248–8254
- Schwartz SE (1989) Sulphate aerosols and climate. *Nature* 340:515–516
- Schwartz SE, Charlson RJ, Kahn RA, Ogren JA, Rodhe H (2010) Why hasn't Earth warmed as much as expected? *J Clim* 23:2453–2464
- Silva AKA et al (2013) Magnetic and photoresponsive theranosomes: translating cell-released vesicles into smart nanovectors for cancer therapy. *ACS Nano* 7:4954–4966
- Swihart MT (2003) Vapor-phase synthesis of nanoparticles. *Curr Opin Colloid Interface Sci* 8:127–133
- Tamborini E, Cipelletti L (2012) Multiangle static and dynamic light scattering in the intermediate scattering angle range. *Rev Sci Instrum* 83:093106
- Tinke AP et al (2008) Particle shape and orientation in laser diffraction and static image analysis size distribution analysis of micrometer sized rectangular particles. *Powder Technol* 186:154–167
- Van de Hulst HC (1957) *Light scattering by small particles*. Dover, New York
- Van Saarloos W (1987) On the hydrodynamic radius of fractal aggregates. *Physica* 147A:280–296
- Veen SJ et al (2012) Colloidal aggregation in microgravity by critical Casimir forces. *PRL* 109:248302
- Wang GM, Sorensen CM (1999) Diffusive mobility of fractal aggregates over the entire Knudsen number range. *Phys Rev E* 60:3036–3044
- Weitz DA et al (1985) Limits of the fractal dimension of the irreversible kinetic aggregation of gold colloids. *Phys Rev Lett* 54:1416–1419
- Wiltzius P (1987) Hydrodynamic behavior of fractal aggregates. *Phys Rev Lett* 58:710–713
- Wiltzius P, Saarloos W (1987) Reply to a comment. *Phys Rev Lett* 59:2123–2126
- Witten TA, Sander LM (1983) Diffusion limited aggregation. *Phys Rev B* 27:5686–5697
- Wyatt P (1993) Light scattering and the absolute characterization of macromolecules. *Anal Chim Acta* 272:1–40

- Yurkin MA, Hoekstra AG (2007) The discrete dipole approximation: an overview and recent developments. *JQSRT* 106:558–589
- Yurkin MA, Hoekstra AG (2011) The discrete-dipole-approximation code ADDA: capabilities and known limitations. *JQSRT* 112:2234–2247
- Yurkin MA, Maltsev VP, Hoekstra AG (2007) The discrete dipole approximation for simulation of light scattering by particles much larger than the wavelength. *JQSRT* 106:546–557
- Zelenyuk A, Cai L, Imre D (2006) From agglomerates of spheres to irregularly shaped particles: determination of dynamic shape factors from measurements of mobility and vacuum aerodynamic diameters. *Aerosol Sci Technol* 40:197–217
- Zhang R, Khalizov A, Wang L, Hu M, Xu W (2012) Nucleation and growth of nanoparticles in the atmosphere. *Chem Rev* 112:1957–2011
- Zimm BH (1948a) The scattering of light and the radial distribution function of high polymer solutions. *J Chem Phys* 16:1093
- Zimm BH (1948b) Apparatus and methods for measurement and interpretation of the angular variation of light scattering: Preliminary results on polystyrene solutions. *J Chem Phys* 16:1099–1116